ELSEVIER

Cardiovascular Research 31 (1996) 917–925

Cardiovascular Research

Effects of afterload on regional left ventricular torsion

Guy A. MacGowan [1], Daniel Burkhoff, Walter J. Rogers, Douglas Salvador, Haim Azhari, Paul S. Hees, Jay L. Zweier, Henry R. Halperin, Cynthia O. Siu, Joao A.C. Lima, James L. Weiss, Edward P. Shapiro *

Division of Cardiology, Johns Hopkins University School of Medicine and the Johns Hopkins Bayview Medical Center, 4940 Eastern Avenue, Baltimore, MD 21224, USA

Received 29 June 1995; accepted 23 January 1996

Abstract

Objective: To determine if left ventricular torsion, as measured by magnetic resonance tissue tagging, is afterload dependent in a canine isolated heart model in which neurohumoral responses are absent, and preload is constant. **Methods**: In ten isolated, blood perfused, ejecting, canine hearts, three afterloads were studied, while keeping preload constant: low afterload, high afterload (stroke volume reduced by approx. 50% of low afterload), and isovolumic loading (infinite afterload). **Results**: There were significant effects of afterload on both torsion ($P < 0.05$) and circumferential shortening ($P < 0.0005$). Between low and high afterloads, at the anterior region of the endocardium only, where torsion was maximal, there was a significant reduction in torsion ($15.1 \pm 2.2°$ to $7.8 \pm 1.8°$, $P < 0.05$). Between high afterload and isovolumic loading there was no significant change in torsion ($7.8 \pm 1.8°$ to $6.2 \pm 1.5°$, P = NS). Circumferential shortening at the anterior endocardium was significantly reduced both between low and high afterload (-0.19 ± 0.02 to -0.11 ± 0.02, $P < 0.0005$), and also between high afterload and isovolumic loading (-0.11 ± 0.02 to 0.00 ± 0.02, $P < 0.05$). Plots of strains with respect to end-systolic volume demonstrated a reduction in both torsion and shortening with afterload-induced increases in end-systolic volume. Torsion, but not circumferential shortening, persisted at isovolumic loading. **Conclusions**: Maximal regional torsion of the left ventricle is afterload dependent. The afterload response of torsion appears related to the effects of afterload on end-systolic volume.

Keywords: Torsion; Afterload; Magnetic resonance tagging; Dog, anesthetized

1. Introduction

During left ventricular ejection, rotation of the apex with respect to the base occurs. This deformation, termed torsion, is due to contraction of obliquely orientated fibres in the epicardium [1], which course towards the apex in a counter-clockwise spiral. Counter-clockwise torsion has important functional consequences. It is transmitted through the entire wall, despite the fact that endocardial fibres spiral in the opposite (clockwise) direction. This results in extensive structural re-arrangement of endocardial myocardium [2,3], and extensive thickening [3]. Furthermore, Arts and coworkers have demonstrated [4,5] that as a result of torsion, fibre shortening and fibre stress are constant through the ventricular wall. In diastole, the shearing forces built up during systole by epicardial and endocardial torsion result in rapid untwisting during isovolumic relaxation, which may contribute to the rapid ventricular filling of early diastole [6,7].

Torsion has been demonstrated with cine-radiography of beads implanted in human transplant recipients at the time of surgery [1], and with magnetic resonance (MR) tissue tagging, a method of non-invasively marking the myocardium [8]. Hansen et al., by studying implanted beads in human transplant recipients, have demonstrated that torsion is sensitive to changes in contractility. Positive

* Corresponding author. Tel. (+1-410) 550-0849; Fax (+1-410) 550-1183.

[1] Present address: Division of Cardiology, University of Pittsburgh Medical Center, 200 Lothrop St., Pittsburgh, PA 152313, USA.

Time for primary review 27 days

PII S0008-6363(96)00042-9

inotropic interventions increase torsion [9,10], while during the early stages of acute allograft rejection there is a reduction in torsion [11]. This finding was particularly interesting as the reduction in torsion during acute rejection was noted before any of the conventional measures of left ventricular function were affected. To determine whether torsion would be a useful method to serially evaluate left ventricular function, Hansen et al. subsequently studied the effects of load alteration. They demonstrated that by volume loading with intravenous fluids, and by pressure loading with methoxamine, there was no effect of load alteration on torsion. The authors thus suggested that torsion may be a relatively load insensitive measure of left ventricular function [10]. Further analysis of a subgroup of the patients from the study of Hansen et al., quantifying twist (defined as the mean longitudinal gradient of torsion with respect to the long axis), also did not demonstrate any effects of methoxamine [12]. These findings were unexpected as torsion results from shortening of epicardial fibres, which would be expected to be load dependent.

However, to conclude that torsion is independent of loading requires further study in ex vivo models. The manipulation of load in human subjects is limited by compensatory mechanisms, which is illustrated by the observation in the study of Hansen et al. that neither alterations in preload or afterload significantly affected stroke volume or ejection fraction [10].

Thus, further studies with independent changes in preload and afterload, to an extent that produces changes in stroke volume, while free of neurohumoral responses, are required to further examine this interesting hypothesis. The isolated, blood perfused, ejecting canine heart preparation is a model which meets these requirements [13]. The heart is completely removed from the chest, so is devoid of neurohumoral responses. Ejection is controlled by a computer programme using the three-element Windkessel model of arterial impedance, with which reproducible, independent changes in afterload can be achieved, within physiological ranges, or between the extremes of loading [14]. In this study MR tissue tagging was used with this model to determine non-destructively the effects of a range of afterloads on regional left ventricular strains, including torsion [8].

2. Methods

2.1.1. Animal preparation

Ten isolated canine hearts were studied. The procedures to isolate and support a canine heart were similar to those described by Suga and Sagawa [14]. For each experiment, a mongrel support dog (mean weight 27.8 ± 3.1 kg) and a mongrel donor dog (mean weight 20.2 ± 1.6 kg) were both anaesthetised with 25–35 mg/kg of pentobarbitol sodium. Additional pentobarbitol sodium was administered during the study to achieve steady anaesthesia. Intravenous heparin (10000 units), hydrocortisone (250 mg), and indomethacin (25 mg), were administered to the support dog, which was mechanically ventilated. The femoral arteries and veins of the larger support dog were cannulated and connected to a system of tubes, and a pump, through which oxygenated arterial blood, under pressure, was supplied to the isolated heart. The chest of the donor dog was opened, the heart removed, and perfused by the oxygenated blood from the support dog via a cannula tied into the left subclavian artery. The venous coronary flow drained into a receptacle, through a vent placed in the right ventricular apex, and via a second pump, was returned to the venous circulation of the support dog through the femoral veins. Any blood collecting in the left ventricle drained through a vent placed in the left ventricular apex. The left atrium was opened, and all the chordae tendineae were freed from the mitral valve leaflets. A plastic ring which holds the isolated heart onto the pump apparatus, was sewn to the mitral valve ring. The left ventricular pressure of the isolated heart was monitored by a fluid-filled catheter placed within the left ventricle which was connected to a Gould electronics pressure transducer. The perfusion pressure of the coronary arteries was monitored by a fluid-filled cannula tied into the aortic root, and the pump in the arterial part of the circulation was adjusted to maintain this pressure at 80 mmHg. The support dog's arterial pressure was continuously monitored, and serial arterial blood gases were taken, and any deficiencies in these were corrected accordingly. ECG leads, and pacing leads for atrial pacing, were sewn onto the heart. To eliminate any possible effect of gravity on the magnitude and regional variation of the measured strains, the heart was placed on the pump apparatus at different orientations for each experiment. Thus, while the heart was always placed horizontally, the anterior region may face up or down.

2.1.2. Control of afterload

The heart, while in the center of the magnetic resonance imaging instrument, contracted against a water-filled balloon placed within the ventricle. This was on the end of a column of water (120 cm long), at the other end of which is a servo pump. A withdrawing motion of the pump's piston allowed the heart at the other end of the apparatus to eject (Fig. 1). The pump, and thus ejection of the isolated heart, was controlled by computer simulation of a hydraulic analogue [15,16] of the three-element Windkessel model of arterial impedance as initially described by Sunagawa et al. [13]. A computer digitised the left ventricular pressure, and computed the instantaneous flow out of the ventricle according to the values of the three parameters that determine the impedance spectrum in this model: the characteristic impedance (R_c), the peripheral arterial resistance (R_a), and arterial compliance (C_a). This flow signal then commanded the servo pump, which withdrew

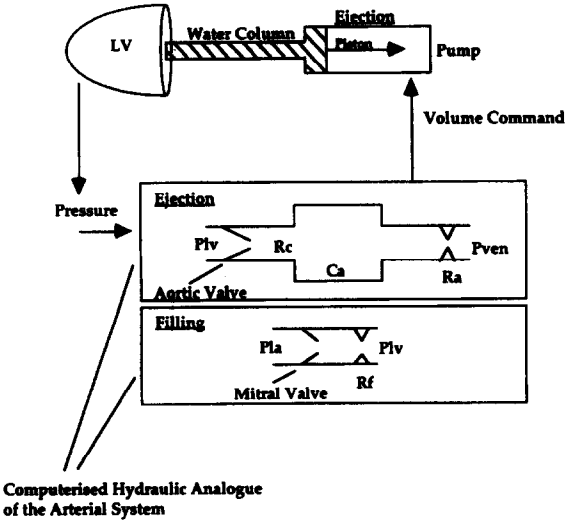

Fig. 1. A diagrammatic representation of the system used to achieve controlled ejection of isolated canine hearts. The hydraulic analogue circuit consists of the left ventricular pressure (P_{lv}), characteristic aortic impedance (R_c), the arterial capacitance (C_a), the peripheral resistance (R_a), and venous pressure (P_{ven}). The filling circuit consists of left atrial pressure (P_{la}), and a filling resistance (R_f).

its piston, allowing ejection. This model has been demonstrated to provide a reasonable representation of input impedance spectra of real arterial systems [17]. By changing the three parameters of this model, afterload can be altered. The ventricle fills during diastole in response to a simple computer-simulated pre-loading circuit consisting of a pressure source (P_{la}) and filling resistance (R_f) [13]. The isolated heart can also be constrained to contract isovolumically, the extreme of afterload.

2.1.3. Experimental protocol

During each experiment two to three different afterloads were studied, in random order. Within each experiment, end-diastolic volume (preload) was kept constant while afterload was changed (Fig. 2). Any change in preload that occurred was corrected by adjusting the filling resistance

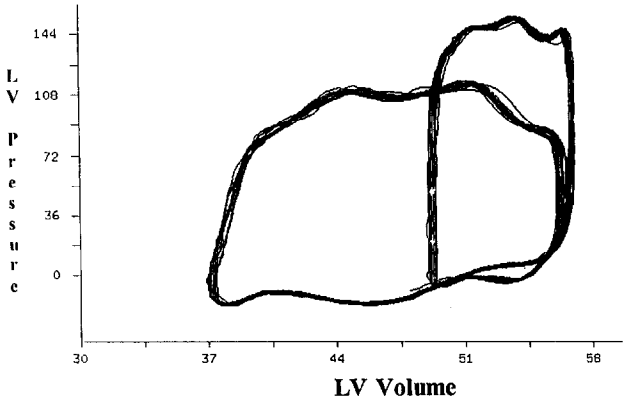

Fig. 2. Pressure volume loops from an isolated, blood perfused, ejecting canine heart contracting against a high and a low afterload, with end-diastolic volume constant.

of the computer-simulated pre-loading circuit. The three interventions were (1) low peripheral arterial resistance (1 $mmHg \cdot s \cdot ml^{-1}$), (2) high peripheral arterial resistance (8 $mmHg \cdot s \cdot ml^{-1}$), and (3) isovolumic contraction (infinite afterload) at the end-diastolic volumes of the ejecting series. The values for low and high afterload were selected based on the changes in stroke volume that they produced, such that stroke volume was reduced by approximately 50% from low to high afterload, a clinically relevant change. Values of the arterial compliance and characteristic impedance were kept constant at 0.1 ml/mmHg and 0.5 $mmHg \cdot s \cdot ml^{-1}$. Stability of the intervention was determined by the left ventricular pressure at the beginning and end of an acquisition of a full set of images. Data were excluded if there was any change in left ventricular pressure of $> 10\%$. This criterion, and poor image quality, were the only criteria used to exclude data.

2.1.4. Magnetic resonance imaging and tissue tagging

MR images were acquired using a Resonex RX4000, 0.38 tesla, resistive iron core magnet. A receiver/transmitter radiofrequency coil surrounded the heart, allowing enhanced image resolution and signal-to-noise ratios [18]. A spin-echo pulse sequence with time to echo (TE) of 30 ms, and time to repeat (TR) of every two RR cycles was used. Four short axis images were acquired at 0.8 to 1.0 cm apart, selected to cover the left ventricle from base to apex. Tags were created by radiofrequency saturation of thin planes orthogonal to the short axis at end-diastole. On each short axis slice, 4 radially spaced tags (transecting the myocardium at 8 locations), intersecting at the center of the left ventricle, were placed at 45° apart (Fig. 3). When acquiring long axis images, the imaging and tagging planes

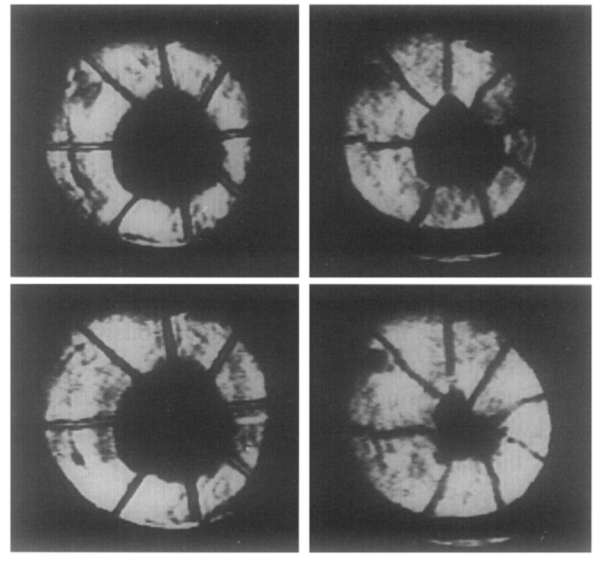

Fig. 3. A series of 4 tagged MR images of isolated, ejecting canine hearts: Top left, End-diastole, high afterload; Top right, End-systole, high afterload; Bottom left, End-diastole, low afterload; Bottom right, End-systole, low afterload. Both end-diastolic images are at the same volume despite different afterloads.

used in the short axis images were interchanged, so that 4 long axis images were obtained at 45° apart, each with 4 transverse tags in the planes previously used to obtain short axis images. Images were acquired at 4 time points. In the ejecting series the 4 time points were at (1) end-diastole (defined as the maximum volume in the isolated heart), (2) peak left ventricular pressure, (3) 80 to 100 ms after peak pressure, and (4) end-ejection (minimum volume). In the isovolumic series, images were acquired at (1) end-diastole, (2) peak pressure, (3) 100 ms after peak pressure, and (4) 200 ms after peak pressure. Torsion was calculated at end-ejection for the ejecting series, and at peak left ventricular pressure for the isovolumic series.

2.1.5. Image analysis

The tag intersection points at the endocardium and epicardium were digitised yielding a set of 8 endocardial and 8 epicardial points per short and long axis slice, using a technique as previously described in detail [7].

2.1.6. Rotational deformations

Rotational deformations were calculated by three different methods to maintain consistency with previous studies [5,6,8,12]. The three methods used were termed (1) Torsion angle, (2) Twist, (3) Angular circumferential-longitudinal shear (Shear CL).

2.1.6.1. Torsion angle. This measurement describes the rotation between base and apex that develops during systole, as described by Buchalter et al. [8]. Two short axis slices were compared, the base and the apical slice. Only end-systolic images were compared, to eliminate rigid body rotation, and to include within the calculation the basal rotation at end-systole which is in the opposite direction to apical rotation. Within each slice, individually for the epicardium and endocardium, the centroid of the 8 tag locations was determined, and the slope of each of these points to the centroid was calculated, and expressed as angles. Torsion was defined as the difference at end-systole in the position of a basal tag point and the corresponding tag point on a succeeding slice expressed as an angle of rotation. Because there was no difference in the relative positions of these two points at end-diastole, the tags being inserted as a plane in both slices simultaneously, this angle represents the rotation of one point with respect to the other point. Increasing angle (positive sign) indicates counterclockwise rotation of the apex when viewed looking towards the base (Fig. 4).

2.1.6.2. Twist. From base to apex, torsion increases in a counterclockwise direction. The gradient of torsion from base to apex is dependent on the torsion angle as calculated above, and also the changes in length between the base and lower slices that occur during systole. For each of the 4 short axis slices, torsion angle (as calculated above)

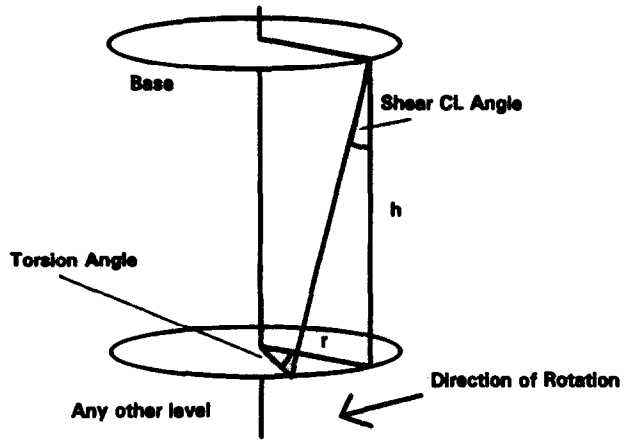

Fig. 4. Diagram illustrating the torsion angle, and the circumferential longitudinal (CL) shear angle (r is the radius, and h is the distance from the apex to base).

and the longitudinal distance of that slice from the base at end-systole were calculated. Linear regression analysis was used to determine the slope of torsion with respect to the length from the base (expressed as degrees/cm). Thus, this measure of left ventricular rotation, as described by Beyar et al. [6] and Moon et al. [12], takes into account the effects of long axis shortening on torsion.

2.1.6.3. Angular circumferential-longitudinal shear (Shear CL). As angular rotation is directly proportional to radius, it is necessary to take this into account when comparing torsion at different cavity volumes, as occurs when afterloads are varied. Shear CL is defined as the difference between the systolic position of an apical tag point and the equivalent tag point on the basal slice as expressed as an angle of which the vertex is the tag point on the basal slice, as previously described by Arts et al. [5], and Buchalter et al. [8]. This angle thus takes into account both radial and longitudinal effects of ejection on torsion, and is calculated according to the formula [8] (Fig. 4):

$$\text{Shear CL} = \tan^{-1}(2r \sin(t/2)/h)$$

where r = radius, t = torsion angle, h = distance between basal and apical slices.

The radius was calculated from the area of the endocardium or epicardium obtained from a computerised contouring system, and h was determined by the distance from the basal tag on long axis images at end-systole.

2.1.7. Three-dimensional reconstruction of tagged data

The endocardial and epicardial tag intersection points from short and long axis images were combined to yield three-dimensional coordinates, using an algorithm as described by Moore et al. [19], and Azhari et al. [20]. Thus, from the combined short and long axis images, 8 tag points at the epicardium, and 8 tag points from the endocardium,

over 4 slices, yielded a set of data with 64 points per time point. The 64 data points formed by the reconstruction of short and long axis images, at each time point, were grouped to yield 24 cuboids.

2.1.8. Finite strain analysis

Finite strain analysis, as originally described by Waldman et al. [2], and identical to the method adapted for MR tagged data by Azhari et al. [20], was applied to the endocardial and epicardial faces of the cuboids. Each cuboid was divided into 4 triangles, and transformed into a regional coordinate system. Strain analysis calculated the circumferential strain, defined as the deformation at end-systole along the tangential direction in the short axis plane with reference to end-diastole, and the longitudinal strain, similarly defined, but in the long axis plane. Subsequently, the principal strain was calculated, defined as the magnitude and direction of the maximal shortening. The direction of the principal strain was expressed as an angle with respect to the circumferential direction, and is a dimensionless number. A negative sign for strain values indicates shortening.

2.1.9. Thickening

Thickening was calculated using a 3-D volume element method as described and validated by Beyar et al. [21], and Lima et al. [22]. Thickness of a cuboid at a given time point was defined as the volume of the cuboid divided by the average surface area of the epicardium and endocardium. The volume of the cuboid was calculated by dividing the cuboid into a series of pyramids, and the endocardial and epicardial surface areas were calculated by dividing these into triangles.

2.1.10. Global left ventricular function

Instantaneous left ventricular volume was read on the computer from the input signal determined by the position of the piston on the servo pump. Stroke volume, end-diastolic volume, and ejection fraction (end-diastolic volume − end-systolic volume/end-systolic volume) were recorded from this signal.

2.1.11. Data analysis

Initially the values from the anterior 4 tags and the posterior 4 tags were averaged. Analysis was focused on the anterior region which was the only area where appreciable values of torsion were demonstrated, which is similar to the method used by Hansen et al. [10]. To allow comparison with the other strains quantified, twist and shear CL were also averaged from the anterior 4 tags and the finite strains and thickening were taken from the anterior 12 cuboids formed by the 3D reconstruction.

Repeated measures analysis of variance was used to determine the effects of afterload on each of the measured strains. Subsequently, the effects of afterload measured between the low and high afterload, and between the high and isovolumic afterloads were determined using Dunnett's multiple comparison procedure. Haemodynamic variables, such as stroke volume and end-diastolic volume were compared between interventions by paired *t*-tests. All results are given as mean ± s.e.m.

These experiments were carried out according to the guiding principles of the institution, and conform with the 'Guide for the care and use of laboratory animals' published by the US National Institutes of Health (NIH publication no. 85-23, revised 1985).

3. Results

3.1.1. Rotational deformations

At the endocardium, torsion and the derived strains twist and shear CL, were maximal at the anterior region (all $P < 0.005$, anterior vs posterior, Table 1). At the epicardium, where values were much lower (Table 2), the differences between anterior and posterior regions were less ($P = 0.06$, anterior vs posterior for torsion; P = NS for twist and shear CL).

Anterior endocardial torsion, and twist, were both significantly affected by the loading interventions (both $P < 0.05$). Between low and high afterloads, there was a significant reduction in torsion from 15.1 ± 2.2° to 7.8 ± 1.8° ($P < 0.05$), and twist from 6.0 ± 0.9°/cm to 3.1 ± 0.8°/cm ($P < 0.05$). Between high and isovolumic loading, there was no significant change in torsion (7.8 ± 1.8° to 6.2 ± 1.5°, P = NS), and twist (3.1 ± 0.8°/cm to 2.3 ± 0.6°/cm, P = NS).

Anterior and posterior endocardial shear CL, and posterior endocardial torsion and posterior endocardial twist were not significantly affected by afterload. While these strains are too low to see statistical differences using our

Table 1
Effects of afterload on regional endocardial rotational deformations (mean ± s.e.m.)

Endocardium		Afterload			ANOVA (*P*)
		Low	High	Isovolumic	
Torsion (°)	Ant.	15.1 ± 2.2	7.8 ± 1.8 *	6.2 ± 1.5	< 0.05
	Post.	4.0 ± 1.9	1.8 ± 2.4	1.5 ± 1.2	NS
Twist (°/cm)	Ant.	6.0 ± 0.9	3.1 ± 0.8 *	2.3 ± 0.6	< 0.05
	Post.	1.7 ± 0.7	1.1 ± 0.7	0.7 ± 0.5	NS
Shear CL (°)	Ant.	4.5 ± 0.6	3.0 ± 0.5	2.4 ± 0.5	= 0.08
	Post.	1.2 ± 1.0	0.8 ± 0.9	0.4 ± 1.0	NS

The 'ANOVA' (analysis of variance) column refers to the significance of the effects of afterload on rotational deformations. Asterisks indicate the significance of the differences between low and high afterload (* $P < 0.05$).
Ant. = anterior; Post. = posterior.

Table 2
Effects of afterload on regional epicardial rotational deformations (mean ± s.e.m.)

Epicardium		Afterload			ANOVA (P)
		Low	High	Isovolumic	
Torsion (°)	Ant.	2.5 ± 1.1	2.4 ± 0.7	2.7 ± 0.9	NS
	Post.	1.2 ± 1.7	0.31 ± 1.3	1.1 ± 1.7	NS
Twist (°/cm)	Ant.	0.9 ± 0.4	0.7 ± 0.3	1.1 ± 0.4	NS
	Post.	0.6 ± 0.7	0.2 ± 0.5	0.5 ± 0.9	NS
Shear CL (°)	Ant.	2.1 ± 0.9	1.9 ± 0.7	2.6 ± 0.8	NS
	Post.	0.9 ± 1.9	0.9 ± 1.4	1.1 ± 2.5	NS

The 'ANOVA' (analysis of variance) column refers to the significance of the effects of afterload on rotational deformations.
Ant. = anterior; Post. = posterior.

methods, anterior endocardial shear CL trended towards significance ($P = 0.08$), and these values were consistent with the significant effects of afterload on anterior endocardial torsion and twist (Table 1). No significant effects on epicardial rotational deformations were seen (Table 2).

3.1.2. Finite strains and thickening

For comparison with torsion, finite strains and thickening were analysed from the anterior endocardium, the only area of the myocardium at which appreciable levels of torsion were detected. Anterior endocardial circumferential, longitudinal, principal strains, and transmural thickening were all significantly affected by the loading interventions (all $P < 0.01$), and these are presented in detail in Table 3. Unlike torsion, circumferential shortening was significantly reduced between the high and isovolumic afterload, as well as between the low and high afterload.

To determine if the responses of the measured strains are related to the effects of afterload on end-systolic volume, strains are plotted against end-systolic volume (Fig. 5). As the strains are quantified in several different units, the afterload response is calculated in terms of percentage with respect to the low afterload. The low

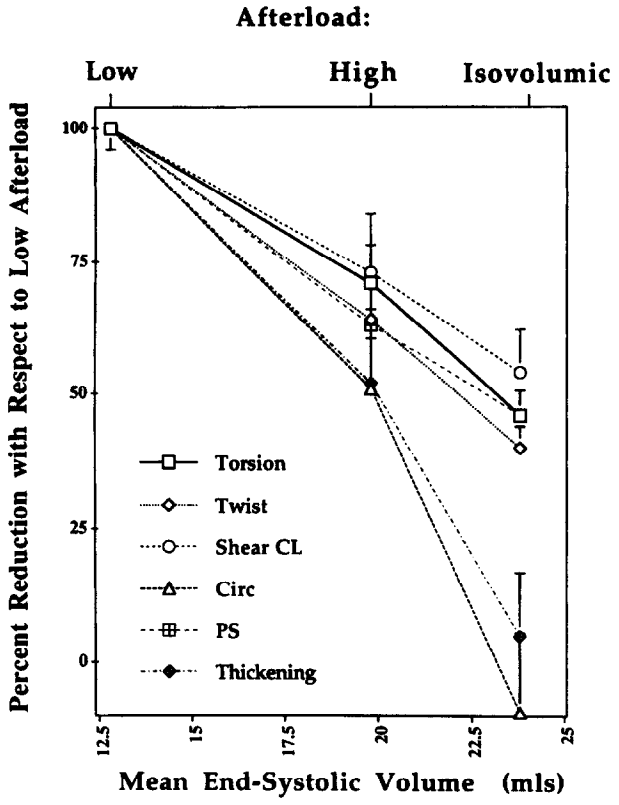

Fig. 5. Diagram illustrating the relation of anterior endocardial strains with increasing afterload. The vertical axis represents the magnitude of strains in terms of percentage with respect to low afterload. Thus, all strains at low afterload are 100%. On the horizontal axis, afterload is quantified in terms of end-systolic volume for each afterload. An additional horizontal axis on the top of the graph indicates the corresponding afterloads. (Circ, circumferential shortening; PS, principal strain.)

afterload is thus 100% for all strains. Mean end-systolic volume at each afterload is on the horizontal axis (without X axis standard errors to aid clarity). As afterload and end-systolic volume are closely related in this preparation, afterload is included as a second X axis on the top of the graph. Only experiments with 3 interventions are included

Table 3
The effects of afterload on anterior endocardial strains and transmural thickening (mean ± s.e.m.)

Endocardium	Afterload			
Strain	Low	High	Isovolumic	ANOVA (P)
Circumferential	−0.19 ± 0.02	−0.11 ± 0.02 ***	0.00 ± 0.02 *	< 0.0005
Longitudinal	−0.04 ± 0.01	0.01 ± 0.02	0.02 ± 0.01	< 0.01
PS	−0.25 ± 0.02	−0.16 ± 0.01 ***	−0.11 ± 0.01 ***	< 0.0005
PS angle (°)	18 ± 5	21 ± 6	30 ± 7	NS
Thickening(%)	21.6 ± 3.0	9.3 ± 1.3 **	0.8 ± 1.7	< 0.0005

The 'ANOVA' (analysis of variance) column refers to the significance of the effects of afterload on strains. Asterisks in the 'High Afterload' column indicate the significance of the differences between low and high afterloads. Asterisks in the 'Isovolumic' column correspond to the significance of differences between high afterload and isovolumic loading (* $P < 0.05$, ** $P < 0.001$, *** $P < 0.0005$).
PS = principal strains; PS angle = principal strain angle (degrees with respect to short axis).

Table 4
The effects of afterload on anterior epicardial strains (mean ± s.e.m.)

Epicardium Strain	Afterload Low	High	Isovolumic	ANOVA (P)
Circumferential	−0.03 ± 0.01	−0.03 ± 0.01	−0.01 ± 0.01	NS
Longitudinal	−0.03 ± 0.01	0.00 ± 0.01	0.02 ± 0.01	= 0.06
PS	−0.11 ± 0.01	−0.08 ± 0.01	−0.08 ± 0.01	= 0.08
PS Angle (°)	42 ± 6	38 ± 7	35 ± 5	NS

The 'ANOVA' (analysis of variance) column refers to the significance of the effects of afterload on strains.
PS = principal strains; PS angle = principal strain angle (degrees with respect to short axis).

($n = 6$). This graph demonstrates that the reduction in rotational and other strains with increasing afterload is related to the increased end-systolic volume. However, there are substantial differences in the magnitude of the strains at isovolumic loading, as circumferential shortening and thickening strains are reduced to a much greater extent than the rotational strains. Note that the principal strain (magnitude of maximal shortening) exhibits a very similar response to the rotational strains, which is consistent with the fact that principal strain includes rotational deformation in its magnitude [20]. Also, the different methods used to calculate rotational deformation, to account for the geometric effects of higher end-systolic volume, do not appear to influence the relationship to end-systolic volume.

Anterior epicardial strains were smaller than those at the endocardium, and the effects of afterload were only of borderline significance for longitudinal shortening and the principal strain ($P = 0.06$, and 0.08 respectively, Table 4). Haemodynamic variables at the various afterloads are described in Table 5. As end-diastolic volumes were not necessarily constant from one experiment to another (though were constant within each experiment), and there were different numbers of interventions at each afterload, this accounts for the non-significant differences in the mean values of end-diastolic volumes between the 3 afterloads (Table 5).

Table 5
Haemodynamics, and the number of experiments (mean ± s.e.m.)

	Afterload Low	High	Isovolumic
LV peak pressure (mmHg)	71.2 ± 6.5	95.7 ± 9.1 *	95.7 ± 11.0 #
LV end-diastolic pressure (mmHg)	−2.5 ± 2.5	0.0 ± 2.0	4.3 ± 2.4
End-diastolic volume (ml)	26.7 ± 4.8	27.2 ± 4.8	23.3 ± 5.8
Stroke volume (ml)	12.6 ± 1.2	5.9 ± 0.6 **	-
Ejection fraction (%)	53.0 ± 3.1	24.6 ± 2.7 **	-
Number	10	9	7

** $P < 0.0001$ high afterload vs. low afterload.
* $P < 0.001$ high afterload vs. low afterload.
# $P < 0.01$ isovolumic vs low afterload.
LV = left ventricular.

4. Discussion

This study was undertaken to determine the effects of afterload on regional left ventricular torsion using a model in which afterload and preload are controlled independently. Contrary to previous studies, the results demonstrate that maximal regional torsion [10], and the derived strain twist [12], are dependent on afterload. The afterload responses of these strains appear related to the effects of afterload on end-systolic volume.

The major effect of afterload in the isolated heart preparation is to increase the end-systolic volume, without affecting the end-diastolic volume (preload). Similarities between this study and others which study volume changes over the cardiac cycle can thus be drawn [6,12]. Using implanted beads in canine studies, Beyar et al. have studied torsion and related this to volume changes (as estimated by radial shortening) during ejection [6]. They demonstrated that torsion is linearly related to volume during ejection. As in the study of Beyar et al. [6], the present study also suggests that torsion increases as end-systolic volume is reduced. Moon et al. have also shown that twist of the human left ventricle is linearly related to volume during systole [12].

The results of this study are also consistent with a recent study from Gibbons Kroeker et al. [23]. They studied the effects of afterload on rotational deformation in the canine model using a novel apical optical device which measures torsion at the apical epicardium. They showed, as in the present study, that twist was affected by afterload, though this was primarily an effect of load on end-systolic volume. The present study further extends the findings of Gibbons Kroeker et al. [23], by measuring total left ventricular torsion rather than solely apical torsion, by demonstrating the marked regional heterogeneity of the afterload response, and by contrasting the different response to afterload exhibited by rotational strains in comparison with circumferential shortening and thickening.

Our study, and the study of Gibbons Kroeker et al. [23] appear to differ in conclusion from the study of Hansen et al. [10]. Those investigators evaluated humans in whom radio-opaque beads had been inserted at the time of cardiac transplantation. No effect of saline-induced preload changes, and methoxamine-induced afterload changes on torsion was found. It was suggested that torsion might be a load-independent measure of the inotropic state. However, altered wedge pressure and blood pressure in Hansen's patients did not change ejection fraction, probably due to mixed preload and afterload effects, and other compensatory mechanisms in these intact human subjects. In contrast marked changes in end-systolic volume and ejection fraction *were* produced in the present study. Our results therefore compliment those of Hansen et al.; load changes without contractility changes *do* effect torsion, but this is through their effects on ventricular volumes.

Since torsion is caused by shortening of counterclock-

wise-spiralling epicardial fibres [1,24], the dependence of torsion on afterload-induced changes in end-systolic volume, as shown in this study is intuitive. However, we have also shown that torsion can persist in an isovolumic preparation, in the absence of shortening, thickening and volume changes. An analogous situation has been demonstrated during the cardiac cycle. Beyar et al., using implanted beads in canine studies [6], and Rademakers et al. [7], using MR tagging, have both demonstrated that rapid recoil of torsion occurs during isovolumic relaxation. This unique behaviour may be an important contributor to the application of restoring forces stored during systole towards the development of suction in early diastole [7,12].

4.1. Advantages and limitations of model

This study involved a novel combination of 2 accepted research techniques: MR tagging has been used to quantify deformation [25] and the isolated, blood perfused, ejecting canine heart model has been used to vary load [13]. MR tagging has a number of advantages. Strains at both the epicardium and endocardium can be sampled at multiple locations throughout the left ventricle [3,20]. The considerable regional variations in the magnitude of torsion emphasise the importance of sampling throughout the left ventricle, which is not possible with implanted radio-opaque markers [1,2,6], or with optical measures of apical twist [23]. MR tags are non-destructive, unlike implanted beads, which may reduce regional perfusion by 25% under acute conditions, and cause the formation of scar around the markers in chronic models [26], which might affect regional function. By acquiring tagged images in 2 orthogonal planes, strains in 3 dimensions can be quantified [19,20], taking into consideration the effects of long axis shortening [27].

The isolated heart model was used for these experiments, since neurohumoral responses to changes in afterload are absent. Furthermore, using this preparation, changes in afterload can be achieved over a wide range, while end-diastolic volume is held constant (Figs. 2 and 3). In the intact circulation an increase in preload would oppose the effects of increased afterload on stroke volume [28], reducing the effectiveness of this intervention. However, the isolated heart model has some non-physiologic aspects which include the fact that the mitral ring is fixed and the chordae tendineae are severed, which could theoretically effect torsion of the left ventricle. However, we have found that the magnitude and regional variations of torsion and other strains described with this model are very similar to those found in closed-chest non-invasive canine studies [20,29]. For example, Rademakers et al. measured shear CL in normal closed-chest dogs, and demonstrated that shear CL was $4.9 \pm 1.1°$ at the anterior region and $1.6 \pm 0.6°$ posteriorly [29]. This compares very closely with values of $4.5 \pm 0.6°$ anteriorly and $1.2 \pm 1.0°$ posteriorly at the low afterload in the present study. Azhari et al. non-invasively measured principal strains in the normal, closed-chest canine heart [20]. They demonstrated that the endocardial principal strain was -0.23 at the anterior region, with a principal strain direction of 29°. This also compares closely with values of -0.25 ± 0.02 and $18 \pm 5°$ at the low afterload in the present study. Thus, these data support the applicability of the isolated, ejecting, canine heart in the quantification of regional strains.

In conclusion we have demonstrated in the isolated, ejecting, blood perfused, canine heart that maximal regional torsion of the left ventricle is afterload dependent. The afterload response of torsion appears related to the effects of afterload on end-systolic volume. The use of this model with MR tagging allows study of the behaviour of regional strains under highly controlled conditions.

Acknowledgements

We are grateful to Stephanie Bosley, Susan Benac, and Kenneth Rent for their invaluable assistance during the course of this study. G.A.McG. is supported by a Knoll/Irish Heart Foundation Fellowship. Supported by NHLBI grants RO1-HL-46223 (EPS), RO1-HL-43722 (JLW), RO1-HL-38324 (JLZ), and RO1-HL-44092 (HRH). Presented in part at the 66th American Heart Association Scientific Sessions, November 1993.

References

[1] Ingels NB, Hansen DE, Daughters GT, Alderman EL, Miller DC. Relation between longitudinal, circumferential, and oblique shortening and torsional deformation in the left ventricle of the transplanted human heart. Circ Res 1989;64:915–927.

[2] Waldman LK, Fung YC, Covell JW. Transmural myocardial deformation in the canine left ventricle. Normal in vivo three-dimensional finite strains. Circ Res 1985;57:152–163.

[3] Rademakers FE, Rogers WJ, Guier WH, et al. Relationship of regional cross-fiber shortening to wall thickening in the intact heart. Circulation 1994;89:1174–1182.

[4] Arts T, Reneman RS, Veenstra PC. A model of the mechanics of the left ventricle. Ann Biomed Eng 1979;7:299–318.

[5] Arts T, Meerbaum S, Reneman RS, Corday E. Torsion of the left ventricle during the ejection phase in the intact dog. Cardiovasc Res 1984;18:183–193.

[6] Beyar R, Yin FCP, Hausknecht M, Weisfeldt ML, Kass DA. Dependence of left ventricular twist-radial shortening relations on cardiac cycle phase. Am J Physiol 1989;257(Heart Circ Physiol 26):H1119–H1126.

[7] Rademakers FE, Buchalter MB, Rogers WJ, Zerhouni EA, Weisfeldt ML, Weiss JL, Shapiro EP. Dissociation between left ventricular untwisting and filling. Accentuation by catecholamines. Circulation 1992;85:1572–1581.

[8] Buchalter MB, Weiss JL, Rogers WJ, Zerhouni EA, Weisfeldt ML, Beyar R, Shapiro EP. Non-invasive quantification of left ventricular rotational deformation in normal humans using magnetic resonance imaging myocardial tagging. Circulation 1990;81:1236–1244.

[9] Hansen DE, Daughters GT, Alderman EL, Ingels NB Jr, Miller DC. Torsional deformation of the left ventricular midwall in human hearts with intramyocardial markers: regional heterogeneity and

sensitivity to the inotropic effects of abrupt rate changes. Circ Res 1988;62:941–952.

[10] Hansen DE, Daughters GT, Alderman EL, Ingels NB, Stinson EB, Miller DC. Effect of volume loading, pressure loading, and inotropic stimulation on left ventricular torsion in humans. Circulation 1991;83:1315–1326.

[11] Hansen DE, Daughters GT, Alderman EL, Stinson EB, Baldwin JC, Miller DC. Effect of acute human cardiac allograft rejection on left ventricular systolic torsion and diastolic recoil measured by intramyocardial markers. Circulation 1987;76:998–1008.

[12] Moon MR, Ingels NB, Daughters GT, Stinson EB, Hansen DE, Miller DC. Alterations in left ventricular twist mechanics with inotropic stimulation and volume loading in human subjects. Circulation 1994;89:142–150.

[13] Sunagawa K, Burkhoff D, Lim KO, Sagawa K. Impedance loading servo pump system for excised canine ventricle. Am J Physiol 1982;243(Heart Circ Physiol 12):H346–H350.

[14] Suga H, Sagawa K. Instantaneous pressure–volume relationships and their ratio in the excised, supported canine left ventricle: Circ Res 1974;35:117–126.

[15] Halperin H, Tsitlik J, Beyar R, Chandra N, Guerci A. Intrathoracic pressure fluctuations move blood during CPR: comparison of hemodynamic data with predictions from a mathematical model. Ann Biomed Eng 1987;15:385–403.

[16] Tsitlik J, Halperin H, Popel S, Shoukas A, Yin FCP, Westerhof N. Modeling the circulation with three-terminal electrical networks containing special nonlinear capacitors. Ann Biomed Eng 1992;20:595–616.

[17] Burkhoff D, Alexander J, Schipke J. Assessment of Windkessel as a model of aortic impedance. Am J Physiol 1988;255(Heart Circ Physiol 24):H742–H753.

[18] Rogers WJ, Zweier JL, Guier WH, Azhari H, Graves WL, Shapiro EP, Weiss JL. High resolution analysis of cardiac deformation using an internal loop gap resonator. S.M.R.M. Book of Abstracts 1991;2:861(Abstract).

[19] Moore CC, O'Dell WG, McVeigh ER, Zerhouni EA. Calculation of three-dimensional left ventricular strains from biplanar tagged MR images. JMRI 1992;2:165–175.

[20] Azhari H, Weiss JL, Rogers WJ, Siu CO, Zerhouni EA, Shapiro EP. Noninvasive quantification of principal strains in normal canine hearts using tagged MRI images in 3-D. Am J Physiol 1993;264(Heart Circ Physiol 33):H205–H216.

[21] Beyar R, Shapiro EP, Graves WL, et al. Quantification and validation of left ventricular wall thickening by a three-dimensional volume element magnetic resonance imaging approach. Circulation 1990;81:297–307.

[22] Lima JAC, Jeremy R, Guier W, et al. Accurate systolic wall thickening by nuclear magnetic resonance imaging with tissue tagging: correlation with sonomicrometers in normal and ischemic myocardium. J Am Coll Cardiol 1993;21:1741–51.

[23] Gibbons Kroeker CA, Tyberg JV, Beyar R. Effects of load manipulations, heart rate, and contractility on left ventricular apical rotation. An experimental study in anesthetized dogs. Circulation 1995;92:130–141.

[24] Buffer SA Jr, Dong SJ, Hees PS, Hutchins GM, Weiss JL, Shapiro EP, Rademakers FE. Predominant influence of epicardial over endocardial fiber angle on the regional variation of left ventricular torsion. Circulation 1994;90:I-13(Abstract).

[25] Zerhouni EA, Parish DM, Rogers WJ, Yang A, Shapiro EP. Human heart: tagging with MR imaging — a method for noninvasive assessment of myocardial motion. Radiology 1988;169:59–63.

[26] Fenton TR, Cherry JM, Klassen GA. Transmural myocardial deformation in the canine left ventricular wall. Am J Physiol 1978;235(Heart Circ Physiol 4):H523–H530.

[27] Rogers WJ, Shapiro EP, Weiss JL, Buchalter MB, Rademakers FE, Weisfeldt ML, Zerhouni EA. Quantification of and correction for left ventricular systolic long-axis shortening by magnetic resonance tissue tagging and slice isolation. Circulation 1991;84:721–731.

[28] Ross J Jr. Afterload mismatch and preload reserve; a conceptual framework for the analysis of ventricular function. Prog Cardiovasc Dis 1976;18:255–264.

[29] Rademakers FE, Meils CM, Rogers WJ, Buchalter MB, Weiss JL, Shapiro EP. Pericardiotomy reverses regional distribution of left ventricular rotational deformation. Eur Heart J 1992;13(supplement):22(Abstract).